Journal of Visualization, Vol. 2, No. 2 (1999) 135-142

Shedding Patterns in Flow-structure Interactions

Evangelinos, C.*, Lomtev, I.* and Em Karniadakis, G.*

* Center for Fluid Mechanics, Division of Applied Mathematics, Brown University, Providence, Rhode Island 02912, USA.

Received 24 March 1999.
Revised 2 June 1999.

***Abstract*:** We use direct numerical simulation (DNS) based on spectral methods and the parallel code *NekTar* to simulate incompressible and compressible flow past flexible structures. Specifically, we consider incompressible turbulent flow past flexible cylinders subject to vortex-induced vibrations (VIV), and compressible flow past a three-dimensional flexible wing subject to insect-like motion. We present several shedding patterns that reveal new oblique shedding modes resembling modulated traveling and standing wave response waves for flexible cylinders as well as strong three-dimensional interactions for flexible wings.

***Keywords*:** turbulent wakes, direct numerical simulations.

1. Introduction

External turbulent flows are very difficult to visualize in numerical simulations despite the fact that strong concentrations of vorticity occur in such flows as wakes, jets, etc. However, when intense three-dimensional interactions take place, as is the case we consider here in flow-structure interactions, the vorticity vector or its magnitude typically provide a rather poor visual representation of the flow dynamics. To this end, in this work we use a new approach in investigating vorticity interactions in incompressible and compressible external flows by tracking appropriate levels of pressure or density surfaces.

In previous work, we used direct numerical simulation to investigate flow-structure interactions in two- and three-dimensions at Reynolds number $Re \leq 300$ [1]. We have used a simple string equation to model the motion of the structure but in [2] we extended that work to flexible beams including the effect of bending stiffness. In the current work, we use the new more efficient code *NekTar* [3], [4], [5] to extend our investigation to higher Reynolds number, where the wake is fully turbulent. In particular, we analyze here results from a simulation at $Re = 1000$ for a flexible cylinder with finite bending stiffness, i.e. a beam whose induced motion resembles either a traveling wave or a standing wave. We also present three-dimensional unsteady simulations of compressible flow past a three-dimensional flapping wing based on a new discontinous Galerkin algorithm developed in [6]. In this case, the motion is not induced by the flow but it is prescribed to follow approximately the stroke of an insect in flight.

In the following, we first review briefly the *NekTar* code and subsequently we proceed with visualizations of each case separately.

2. Simulation and Visualization Methods

2.1 The NekTar Code

Spectral discretizations have been very effective in direct numerical simulations of homogeneous turbulence and shear turbulence in simply-connected and separable domains (e.g. channel flow). The first generation of spectral

element methods extended spectral accuracy to more complex domains but was limited to relatively simple domains and structured grids [7]. The new generation of spectral methods extends the application of these methods to unstructured and hybrid grids [4], [5]. High-order accuracy is particularly important in long-time integration of the Navier-Stokes equations such as turbulence simulation, where hundreds of thousands of time-steps are needed for each simulation in order to achieve converged statistics.

NekTar is a suite of codes based on this new generation of spectral/hp element methods [8]. There are several variations of these codes appropriate for different flow models and geometries, i.e., for incompressible, compressible, and plasma flows. The first version *NekTar* -F incorporates two-dimensional quadrilateral and triangular elements with Fourier expansions along the third (cartesian or azimuthial) direction. A straightforward mapping of Fourier modes to P processors results in an efficient and balanced computation where the three-dimensional problem is decomposed into two-dimensional problems (linear Helmholtz solves in Navier-Stokes equations) and multiple one-dimensional FFTs (nonlinear contributions in Navier-Stokes equations). The implementation of *NekTar* -F on different platforms using rigorously defined benchmark problems is given in Crawford et al. (1996) [9] and more recent developments in Evangelinos et al. (1999) [10]. The parallelization of the more general code is more complicated. It is based on a multi-level graph decomposition method developed at University of Minnesota [11], which we extended so that it suits the specific characteristics of the spectral/hp method implemented in the *NekTar* code.

For the simulations presented here, we first used the *NekTar* -F code in conjunction with a geometry-fitted technique and an appropriate three-dimensional mapping to compute the incompressible flow past a freely vibrating flexible cylinder. For the compressible flow simulations past a flexible wing we used the *NekTar* -ALE version, which is based on a discontinuous Galerkin algorithm [6] and the arbitrary Lagrangian-Eulerian formulation (ALE) that provides great flexibility in discretization. Specifically, the grid is updated using a fast algorithm inspired by graph theory and the so-called force-directed method [12].

2.2 Visualization Approach

NekTar uses unstructured and hybrid domains, which lead to a distribution of output data in a very non-uniform grid. Most available visualization packages suffer from severe accuracy degradation when handling data in non-uniform grids. To this end, we first interpolate the output of *NekTar* using spectral interpolations on a uniform grid by respecting the dynamic changes in the geometry, and subsequently we perform the visualizations.

We are interested in studying the near-wake vorticity dynamics and so vorticity visualization is a standard approach used. While this is useful and admits a fairly simple interpretation in two-dimensions, in three-dimensions vorticity visualizations are substantially more difficult to perform and to interpret. For example, if vorticity magnitude is used as a scalar quantity to visualize the near-wake in flow-structure interactions, important details of the dynamics cannot be presented. Instead, we can use iso-surfaces of pressure at appropriate levels to visualize details of the wake. A more accurate approach is to find the vortex cores using the approach pioneered by Jeong and Hussain [13] based on the eigenvalues of the velocity gradient tensor, but this is rather costly.

To contrast the visualization results obtained using the different methods, we plot in Fig. 1 iso-surfaces of vorticity magnitude at two different values, and pressure iso-surfaces. In particular, we employ a solid surface at a minimum (negative value) and another grid surface at a value slightly above the previous one. To demonstrate that the iso-pressure surfaces so tracked are representative of the corresponding vorticity dynamics, we also plot in Fig. 1 a similar plot of the spanwise vorticity following the same two-surface tracking approach, as before. We see that indeed the pressure iso-surface and the spanwise vorticity iso-surfaces present the same instantaneous picture in the near-wake. We also include a plot of the iso-contour of the second largest eigenvalue following the technique of Jeong and Hussain [13], which shows the resemblance with the other plots but it is not as informative as the pressure iso-surface plot. Unlike the pressure iso-surface which is a continuous manifold and thus can clearly reveal complicated vortex structure interactions, the other surfaces are not continuous manifolds and provide somewhat less detail. This is true for open flows (vortex-dominated) but not necessarily for wall-bounded flows. It is also more efficient to follow pressure iso-surfaces than vorticity iso-surfaces, so in the following we will adopt the former approach in the case of incompressible flow, and the tracking of density iso-surfaces in the case of compressible flow.

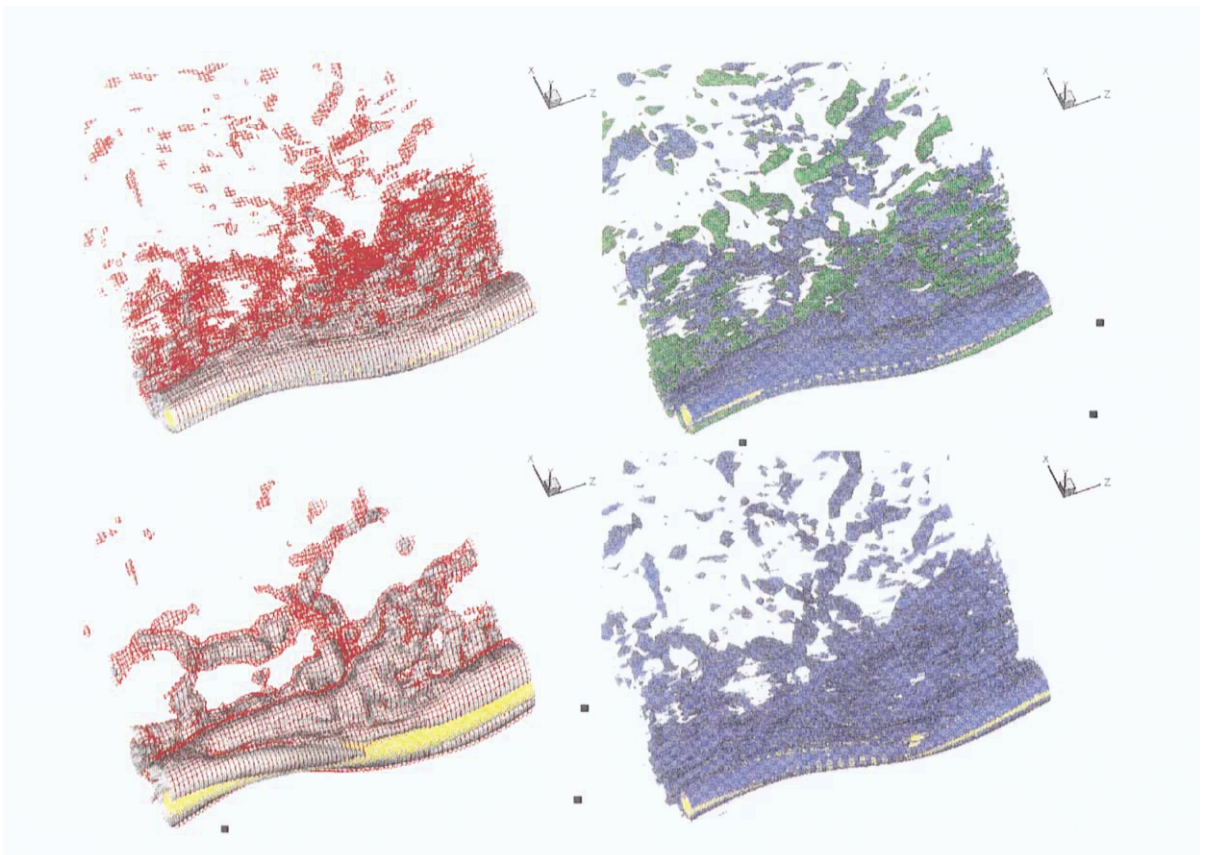

Fig. 1. DNS of flow past a flexible beam at Reynolds number 1,000. Top left: Total vorticity magnitude at levels 3.0 and 5.5; Top right: Spanwise vorticity at −1.7 and 1.7; Bottom left: Pressure iso-surfaces at −0.18 and −0.24. Bottom right: Iso-contour at −1.3 of the second largest eigenvalue using the technique of Jeong and Hussain (1995). All values are non-dimensionalized with respect to the flexible cylinder diameter and the freestream velocity.

3. Incompressible Flow Past a Flexible Cylinder

3.1 Simulation Parameters

We report first results from DNS for uniform flow past a flexible cylinder, subject to vortex-induced vibrations (VIV) at Reynolds number $Re = 1000$ and mass ratio of 2 (cylinder mass over displaced fluid mass), which is a typical value for VIV in water. The Reynolds number is defined based on the cylinder diameter D and the free stream velocity U. In all cases we neglect the structural damping as we are interested in the maximum amplitude response. We also allow only vertical motions in the crossflow y-direction, i.e., we do not allow any motion in the streamwise x-direction. We have chosen the structure eigenfrequency to be equal to the Strouhal number of the corresponding stationary cylinder flow as we are interested in lockin states only. The governing equations are the incompressible Navier-Stokes equations coupled with the equation of the structure dynamics, i.e., the beam equation.

3.2 Flow Vizualizations

To contrast low Reynolds number shedding with shedding at $Re = 1000$ we first plot in Fig. 2 pressure isocontours at $Re = 300$ for the freely oscillating rigid cylinder. We see that shedding is parallel in the near-wake and that the first strong interaction occurs at a location $x/D \approx 10$. The near-wake also appears two-dimensional up to that location. The corresponding shedding pattern is of the type $2S$ as in the low Reynolds number two-dimensional simulations. Here we use the terminology established by Williamson and Roshko (1988) [14].

At Re = 1000 the vortex tubes shown clearly in the low Reynolds number simulations are very deformed and are only visible in the very near-wake. For the stationary cylinder (not shown here) the shedding is nominally parallel, although there is substantial three-dimensional structure in the form of small cells along the span [15]. For the rigid freely oscillating cylinder shown in Fig. 2 shedding is also parallel, and by examining several slices of the flow along the span we identify a 2 P pattern. Therefore, there is a switch from the 2 S mode to a 2 P mode as the Reynolds number increases, similar to the qualitative change in the two-dimensional simulations, and in accord with the visualizations of Sheridan et al. [16]

For a flexible cylinder with periodic ends (in the span) vortex shedding at Re = 1000 has changed significantly compared to the low Reynolds number states. A modulated traveling wave describes approximately the induced motion of the cylinder. In Fig. 3 we plot pressure isocontours of the flow at two different instances. We see that part of the wake corresponds to parallel shedding, similar to the rigid cylinder, and part corresponds to oblique shedding at an angle of about 30 degrees. These as well as other flow visualizations not shown here (see [15]) suggest that the onset of oblique shedding coincides with a node which is traveling along the span. In particular, the phase speed is detected by following the motion of the vibrating structure (i.e., the cable) that for this particular case undergoes a free oscillation resembling a traveling wave. This creates a discontinuity in phase or a vortex dislocation (see Williamson, 1996 [17]), which causes vortex filaments to turn with respect to the axis of the cable resulting in oblique shedding. These vortex filaments produce patterns similar to what have been termed as phase shocks by Miller and Williamson (1994) [18] who have created such structures experimentally using variable suction at the ends of a stationary cylinder.

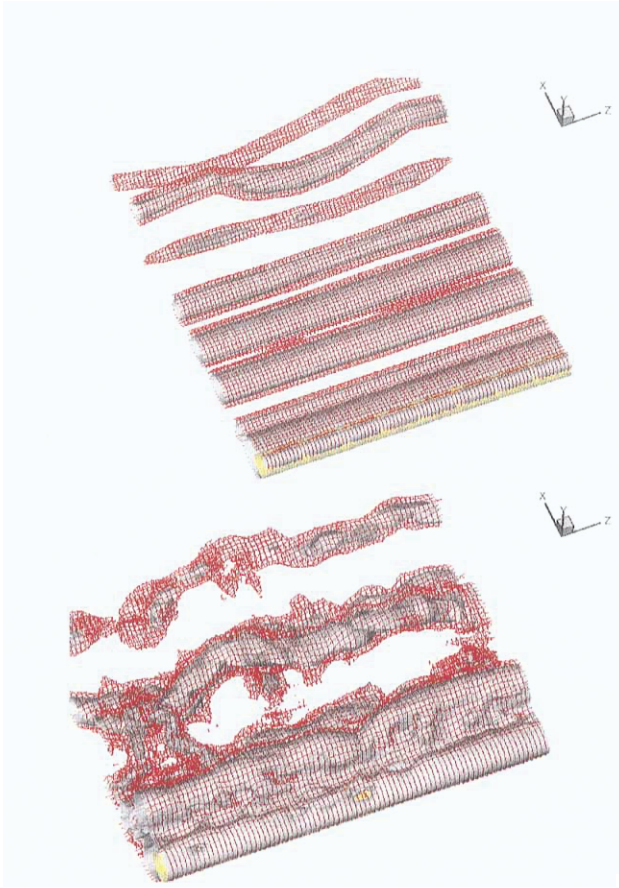

Fig. 2. Rigid cylinder: Top ; Re = 300 and pressure isocontrours at values −0.3 and −0.4. Bottom ; Re = 1000 and pressure isocontrours at −0.2 and −0.3.

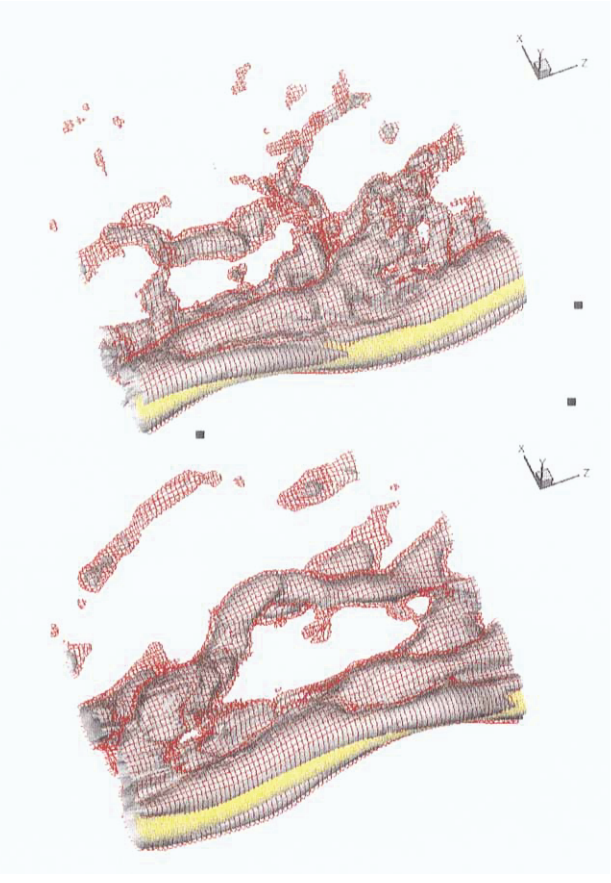

Fig. 3. Traveling was response at Re = 1000: Top ; Pressure isocontours at values −0.24 and − 0.18 (t = 490.09). Bottom ; Pressure isocontrours at values −0.24 and −0.18 (t = 532.09).

There is, however, a difference with the structures in our visualizations; unlike the experiment of Miller and Williamson (1994) [18] where the discontinuity point is fixed, here it coincides with the node, which is moving with the phase speed along the span of the cable or beam. In the experiments with the stationary cylinder, therefore, the inclined vortex filaments are located towards one side of the cylinder, whereas in the beam simulations the inclined filaments alternate sides.

A fundamentally different pattern is produced if the end points of the flexible cylinder in the span are fixed. In this case, a standing wave describes approximately the motion of the flexible cylinder. In Fig. 4 we plot instantaneous pressure contours as before. The shedding patterns for this case are different than before, as the vortex tubes shed off the cylinder are bent towards the flow direction with fixed vortex dislocations at the two fixed nodes along the span.

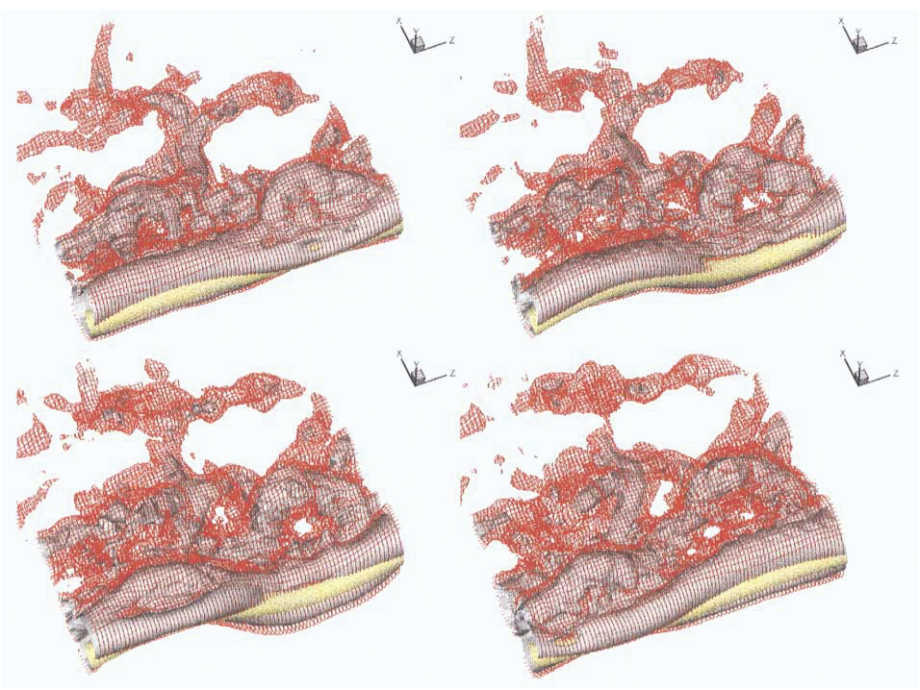

Fig. 4. Standing wave response at Re=1000: Pressure isocontoursat values -0.1 and -0.2. The different snapshots correspond to times one-fifth of the shedding cycle apart (top-left; top-right; bottom-left; bottom-right).

4. Compressible Flow Past a 3D Flapping Wing

4.1 Simulation Parameters

Here we use the *NekTar* -ALE code to simulate compressible flow past a 3D flapping wing subject to insect-like motion. Specifically, we consider the flow past a three-dimensional wing formed by a prismatic NACA 4420 airfoil placed at 20 degrees angle of attack. Two-dimensional subsonic and supersonic simulations were presented in [6]. In particular, we consider the wing moving according to

$$u = 0; \quad v = A\cos(2\pi ft)\, H(z - z_0)\, 2(z - z_0)/(Lz/2); \quad w = 0$$

where z runs along the span of the airfoil, $z_0 = 2.5$ is the reference point, $L_z = 5$ is the spanwise length of the airfoil, $A = 0.5$ is the amplitude of the motion, and f is the frequency with $2\pi f = 1.57$; also $H(z)$ is the Heaviside function. The motion we simulate resembles in some general way the flapping motion characteristic of insect flight [19].

We have performed simulations at chord Reynolds number $Re = 680$ and Mach number $M = 0.3$. The discretization consists of 15,870 tetrahedra of $p = 3$ polynomial order and the time step was taken $\Delta t = 0.00025$.

The origin of the reference frame is at the midpoint of the airfoil and the domain extends from $x = -2.5$ at the inflow to $x = 7.5$ at the outflow and from $y = -2.5$ to $y = 2.5$ at the sides. Here the non-dimensionalization is with respect to the chord length ($C = 2$ in our computations) and the freestream velocity ($U_\infty = 1.75$ in our computations).

In Fig. 5 we plot the lift and drag coefficients versus time, and we compared them with the corresponding

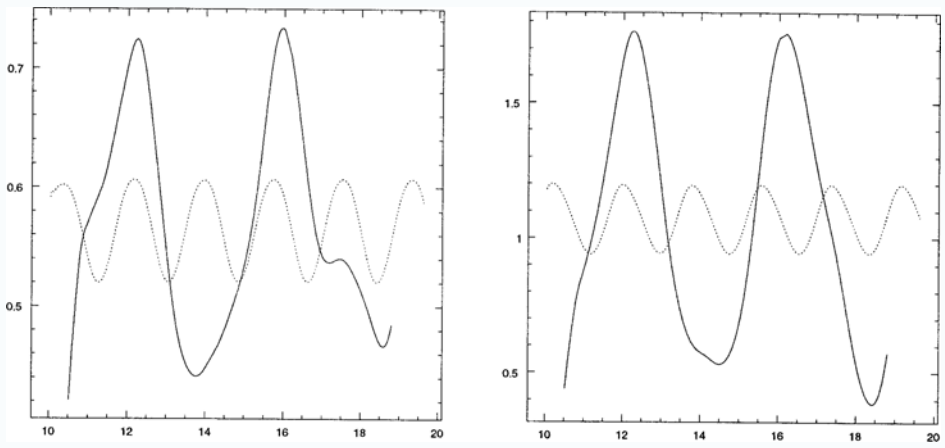

Fig. 5. Drag (left) and lift (right) coefficients versus time for the 3D flapping wing. The dot line denotes force of the corresponding two-dimensional simulation and the solid line show the simulation results of the 3D flapping wing.

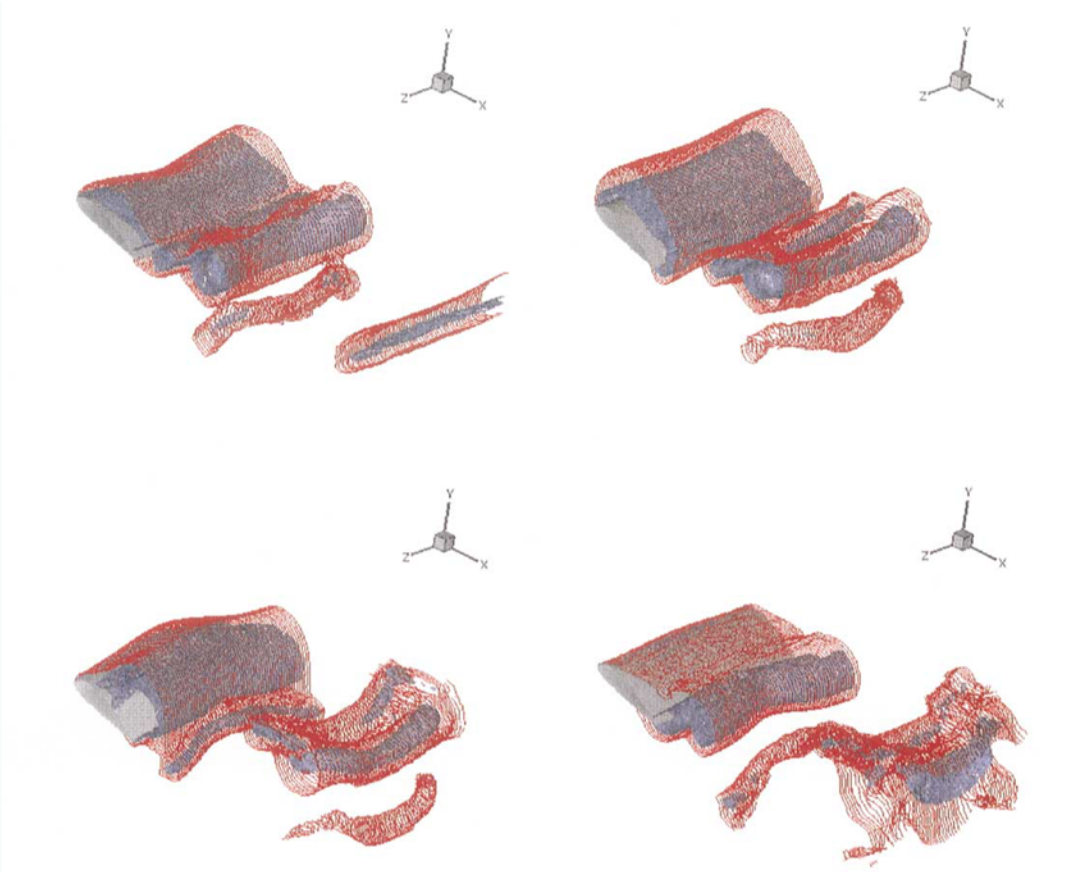

Fig. 6. Top Left: Density contours from the 3D flapping wing simulation corresponding to time $t = 15.5$; Top Right: 16.3; Bottom Left: 17.5; Bottom Right: 18.4. (The simulation with flapping started at $t = 10.36$ from a simulation with the stationary configuration and the flapping period is 4 in non-dimensional units.)

coefficients from exactly the same airfoil but in two-dimensional flow at the same angle of attack. The time variation is due to natural vortex shedding in this case. It is interesting to note that instantaneous values of the lift-over-drag ratio can be increased by about 25% compared to the time-averaged valued, with the latter close to the value obtained from the corresponding two-dimensional simulations.

4.2 Flow Visualizations

Next we present a sequence of flow visualizations during one flapping cycle in Fig. 6. We use minima of density contours to capture the vortex tubes that are shed off the flapping wing. We see that there seems to be a clear lag between the motion of the flapping wing and the visualized vortex tubes. The flapping motion essentially re-arranges the vortex street resulting in a very different lift and drag force distribution. To examine qualitatively this difference we plot in Fig. 7 instantaneous contours of density first from the two-dimensional simulation (left) and also from the three-dimensional simulation at the mid-plane (right). We see that in the former case a regular von Karman vortex street is formed, but in the latter an irregular secondary vortex street is developed downstream. The three-dimensional visualizations show that deformed vortex tubes produced by the flapping motion of the wing are subject to strong interactions even in the near wake, more so than the vortex tubes shed off a stationary wing [20].

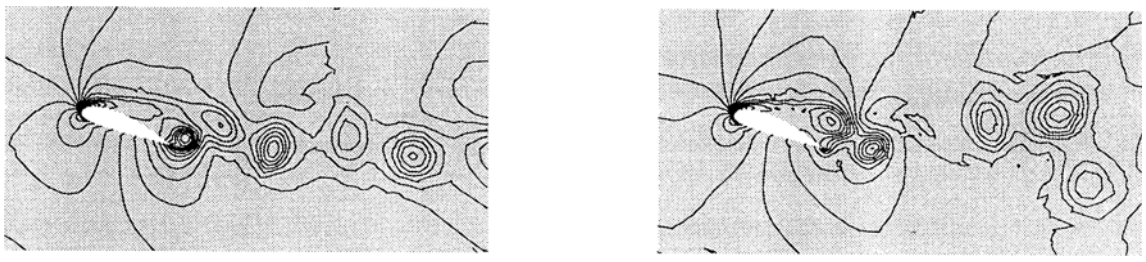

Fig. 7. Instantaneous density contours comparing the structure of vortex street for the two-dimensional simulation (left) and a mid-plane “slice” of the three-dimensional simulation (right). For the three-dimensional simulation the time instance is the same as the bottom left image in Fig. 6.

5. Summary

We have presented here direct numerical simulations of flow-structure interactions for both incompressible and compressible flows. Visualizing unsteady three-dimensional open flows is a very difficult task as spatially developing flows require typically one order of magnitude more degrees of freedom compared to, for example, turbulent flows in periodic channels. To this end, hierarchical methods like the one presented here based on spectral discretization with multi-resolution capabilities, make this task more efficient.

In addition to the computational and data management complexities, no established way exists to visualize wake flows, especially in the mixed laminar-turbulent regime as is the case presented here for the incompressible flow past a flexible cable at $Re = 1000$. To this end, four different methods were tested and it was shown that pressure iso-surfaces could be used in conjunction with the technique of Jeong and Hussain (1995) to follow the complicated vortex tube dynamics present in flow-structure interactions. This was demonstrated also for the compressible wake past a three-dimensional wing subject to insect-like motion. Unlike iso-surfaces of other quantities, pressure iso-surfaces form continuous unsteady two-dimensional manifolds that can be accurately and efficiently followed in-time. In particular, the method of introducing two pairs of iso-surfaces proposed in this paper eliminates some of the artifacts associated with arbitrary thresholds and offers a more lively representation of vortex dynamics encounered in the very important engineering applications of flow-structure interactions. Such dynamics has been relatively unexplored so far and the current paper is a first attempt towards this goal.

Acknowledgments

This work was supported by the Office of Naval Research, the Air Force Office of Scientific Research, and the Department of Energy. Computations were performed on the O2000 at NCSA, on the T3E at NAVO, and on the SP2 at Maui High Performance Computing Center.

References

[1] D. J. Newman and G. E. Karniadakis. Simulations of flow past a freely vibrating cable. Journal of Fluid Mechanics, 344: 95-136, 1997.
[2] C. Evangelinos and G. E. Karniadakis. Transition in the wake of flexible cables and beams. In 7th ISOPE Conference, Honolulu , Hawaii, 1997.
[3] S. J. Sherwin and G. E. Karniadakis. A triangular spectral element method; applications to the incompressible Navier-Stokes equations. Comp. Meth. Appl. Mech. Eng., 23: 83, 1995.
[4] S. J. Sherwin and G. E. Karniadakis. Tetrahedral hp finite elements: Algorithms and flow simulations. Journal of Computation al Physics, 122: 191, 1996.
[5] T. C. Warburton. Spectral/hp Element Methods on Polymorphic Multi-Domains: Algorithms and Applications. PhD thesis, Division of Applied Mathematics, Brown University, 1998.
[6] I. Lomtev, C. Quillen, and G. E. Karniadakis. Spectral/hp methods for viscous compressible flows on unstructured 2D meshes. J. Comp. Phys., 144: 325-357, 1998.
[7] G. E. Karniadakis, E. T. Bullister, and A. T. Patera. A spectral element method for solution of two- and three-dimensional t ime-dependent incompressible Navier-Stokes equations. In Proc. Europe-U.S. Conference on Finite Element Methods for Nonlinear Problems, Sprin ger-Verlag, 803, 1985.
[8] G. E. Karniadakis and S. J. Sherwin. Spectral/hp Element Methods in CFD. Oxford University Press, New York, New York, 1999.
[9] C. H. Crawford, C. Evangelinos, D. J. Newman, and G.E. Karniadakis. Parallel benchmarks of turbulence in complex geometries. Computers and Fluids, 25: 677, 1996.
[10] C. Evangelinos, S.J. Sherwin, and G.E. Karniadakis. Parallel DNS algorithms on unstructured grids. Comp. Meth. Appl. Mech. Engr., special issue on Vistas in Domain Decomposition and Parallel Processing in Computational Mechanics, (ed.) C. Farhat, in press.
[11] G. Karypis and V. Kumar. METIS: Unstructured graph partitioning and sparse matrix ordering system version 2.0. Technical report, Department of Computer Science, University of Minnesota, Minneapolis, MN 55455, 1995.
[12] G. Di Battista, P. Eades, R. Tamassia, and I. G. Tollis. Graph Drawing. Prentice Hall, 1998.
[13] J. Jeong and F. Hussain. On the identification of a vortex. Journal of Fluid Mechanics, 285: 69-94, 1995.
[14] C. H. K. Williamson and A. Roshko. Vortex formation in the wake of an oscillating cylinder. Journal of Fluids and Structure s, 2: 355-381, 1988.
[15] C. Evangelinos. Parallel Simulations of Vortex-Induced Vibrations in Turbulent Flow: Linear and Non-Linear Models. PhD thes is, Division of Applied Mathematics, Brown University, 1999.
[16] J. Sheridan, J. Carberry, J. -C. Lin, and D. Rockwell. On the near-wake topology of an oscillating cylinder. Journal of Flu ids and Structures, 12: 215-220, 1998.
[17] C. H. K. Williamson. Vortex dynamics in the wake. Annual Review of Fluid Mechanics, 28: 477-539, 1996.
[18] G. D. Miller and C. H. K. Williamson. Control of three-dimensional phase dynamics in a cylinder wake. Experiments in Fluids, 18: 26, 1994.
[19] H. Liu and K. Kawachi. A numerical study of insect flight. J. Comp. Phys., 146: 124-156, 1998.
[20] I. Lomtev. Discontinuous Spectral/hp Element Methods for High Speed Flows. PhD thesis, Applied Mathematics, Brown University, 1999.

Authors' Profiles

Constantinos Evangelinos: He received his B.Sc. from Cambridge University in 1993, and his Ph.D. from Brown University in 1999, both in Applied Mathematics. His research interests are in parallel computing and direct numerical simulation of flow-structure interactions.

Igor Lomtev: He received his M.Sc. from Moscow State University in 1991 and his Ph.D. from Brown University in 1999, both in Applied Mathematics. His work has contributed to the development of discontinuous Galerkin spectral methods for compressible viscous flows.

George Em Karniadakis: He received his M.Sc. and Ph.D. from Massachusetts Institute of Technology in 1984 and 1987, respectively, both in Mechanical Engineering. He did his postdoc at Stanford University, and he previously taught at Princeton University. He is currently Professor of Applied Mathematics at Brown University. He has pioneered spectral methods on unstructured grids and parallel simulations of turbulence in complex geometries.